# Low-lying quasibound rovibrational states of H₂ ¹⁶O**

Tamás Szidarovszky [a] & Attila G. Császár [a]

[a] Laboratory of Molecular Structure and Dynamics, Institute of Chemistry , Eötvös University , H-1518, Budapest 112 , P.O. Box 32 , Hungary
Accepted author version posted online: 14 Apr 2013.Published online: 10 May 2013.

PLEASE SCROLL DOWN FOR ARTICLE

Taylor & Francis
Taylor & Francis Group

# INVITED ARTICLE

## Low-lying quasibound rovibrational states of $H_2{}^{16}O$**

Tamás Szidarovszky and Attila G. Császár*

*Laboratory of Molecular Structure and Dynamics, Institute of Chemistry, Eötvös University, H-1518 Budapest 112, P.O. Box 32, Hungary*

A complex coordinate scaling (CCS) method is described allowing the quantum chemical computation of quasibound (also called resonance or metastable) rovibrational states of strongly bound triatomic molecules. The molecule chosen to test the method is $H_2{}^{16}O$, for which an accurate global potential energy surface, a previous computation of a few resonance states via the complex absorbing potential (CAP) method, and some Feshbach ($J = 0$, where $J$ is the quantum number characterising overall rotations of the molecule) and shape ($J \neq 0$) resonances measured via a state-selective, triple-resonance technique are all available. Characterisation of the computed resonance states is performed via probability density plots based on CCS rovibrational wavefunctions. Such plots provide useful details about the physical nature of the resonance states. Based on the computations and the resonance plots, the following useful facts about the resonance states investigated are obtained: (a) Feshbach resonances are formed by accumulation of a large amount of energy in either the non-dissociative bending or symmetric streching modes, excitations by more than five quanta are not uncommon; (b) there are several resonance states with low and medium bending excitation, the latter are different from the states observed somewhat below dissociation by the same triple-resonance technique; (c) several types of dissociation bahavior can be identified, varying greatly among the states; (d) several pairs of $J = 0$ and $J = 1$ Feshbach resonance states can be identified which differ by rigid-rotor type energies; and (e) the lifetimes of the assigned $J = 1$ rovibrational Feshbach resonances are considerably longer than the lifetimes of their $J = 0$ vibrational counterparts.

**Keywords:** complex absorbing potential (CAP); complex coordinate scaling (CCS); water molecule; Feshbach and shape resonances; probability density plots; tunneling

## 1. Introduction

An important characteristics of the fourth age of quantum chemistry [1] is the method development related to nuclear motion theory. A considerable challenge of such efforts is the advancement of non-Hermitian techniques of computational quantum chemistry [2]. These techniques find many applications in atomic and molecular physics and chemistry [2–6], including unimolecular reactions, photodissociation and photoassociation studies, and scattering phenomena. Furthermore, they can be immediately applied in high-resolution molecular spectroscopy to improve our understanding and modeling of the quasibound (ro)vibrational states (also known as resonances or metastable states) of molecules, the principal topic of this paper.

Quasibound or metastable states of molecular systems have sufficient energy to brake up the system into subsystems. Such resonance states decay exponentially with time. While a rigorous mathematical theory of quasibound states does exist [7,8], resonance phenomena can also be approached in a much more intuitive manner, still providing

useful tools for a variety of practical applications. For example [9,10], in the Schrödinger representation resonance states can be associated with outgoing eigenfunctions of the Hamiltonian, diverging exponentially at infinity. Due to the outgoing boundary condition, resonance states are characterised by complex eigenvalues. They are usually written as $E_n^{res} = \varepsilon_n - \frac{i}{2}\Gamma_n$, where $\varepsilon_n = \text{Re}(E_n^{res})$ is the resonance energy (with respect to the ground-state energy of the system) and $\Gamma_n$ is the width of the resonance state, related to the inverse lifetime at a given **q** point in coordinate space by $\rho_n(\mathbf{q}, t) \propto e^{-\Gamma_n t}$ (in atomic units), where $\rho_n(\mathbf{q}, t) = |\Psi_n^{res}|^2$ and $\Psi_n^{res}$ is the $n$th resonance wavefunction.

In order to reach the goal of computing quasibound (ro)vibrational states and to understand near-dissociation high-resolution molecular spectra, one possible approach among several [11,12], and the one pursued here, starts with the computation of all the bound states of the molecule. For strongly bound triatomic molecules even this task requires a substantial amount of work both via electronic structure and nuclear motion computations [1].

---

To construct a potential energy surface (PES) which is accurate globally, i.e. all the way to the first dissociation limit, is by itself a significant challenge, which has been met for only a few molecules, for example, for the ground electronic states of $H_2O$ [13,14], $H_3^+$ [15], and HOCl [16]. Two related issues are noted. The first difficulty when trying to construct a PES having correct dissociative behaviour is the accurate computation of the great many energy values far away from equilibrium, where usually several electronic states come close to each other. Therefore, one may need to resort to multireference methods of electronic structure theory [17]. Computation of adiabatic Born–Oppenheimer (BO) energy corrections (usually called DBOC) [18] with multireference wavefunctions is not a standard technique yet. Even if one is capable of producing the large number of accurate PES points, which cover the coordinate space sufficiently densely, a second difficulty arises, namely the fitting of an analytical functional form to the energy points toward the asymptotic region with high accuracy. This is also a more or less unresolved task at present.

If an accurate global PES is at hand, the next step is the computation of the *bound* rovibrational states up to dissociation, as they also have a substantial interest. In order to compute the usually thousands of bound rovibrational states, one needs to use an effective algorithm which is capable of describing the diffuse, highly excited states where the best choice of basis functions is less clear. Another difficulty in computing highly excited states arises from singular terms always present [19] in tailor-made Hamiltonians [20] based on internal coordinates. If the so-called singular nuclear configurations, corresponding to singularities present in the kinetic energy operator, are energetically accessible by the nuclear motions investigated, special care must be exercised to avoid the resulting numerical problems during the variational computation of (ro)vibrational states. Theoretical techniques that do not treat these singularities may result in unconverged eigenenergies; therefore, these methods cannot be employed when the goal is the determination of the complete (ro)vibrational spectrum. An efficient algorithm developed in our group for triatomic rovibrational computations up to dissociation is the $D^2FOPI$ (mixed discrete variable (DVR) [21] and finite basis (FBR) [21] representation of the rovibrational Hamiltonian expressed in orthogonal internal coordinates using a direct product basis and an iterative eigensolver) algorithm. It is described for the vibrational case in Ref. [14] and in more detail, including the rovibrational case, in Ref. [22]. In previous studies the $D^2FOPI$ code has been shown to be capable of computing (nearly) all the bound vibrational states of the $H_3^+$ and $H_2^{16}O$ molecules [13,14].

This work is aimed at developing an efficient algorithm and computer code capable of yielding a large number of rovibrational resonances of strongly bound triatomic molecules. In order to be able to compute resonance states, which have asymptotically exponentially diverging wave-functions, with the well-developed variational methods of quantum chemistry based on square-integrable functions, one needs to have some additional techniques to overcome the complexity introduced by the asymptotic behaviour. There are several algorithms explored in the past decades to achieve this, see, for example, Ref. [2] and the introduction of Ref. [23].

In this study (ro)vibrational resonances are computed by merging the $D^2FOPI$ algorithm, based on square-integrable functions, with the complex coordinate scaling (CCS) method. The CCS technique has been used in molecular physics and computational chemistry for several decades. Excellent application-oriented reviews [10,24,25] can be found along with discourses on the rigorous mathematical foundations of complex scaling [26–29]. Over the years several variants of the 'conventional' complex scaling method were proposed, such as the exterior complex scaling [10,30] or the smooth exterior complex scaling [10,31], from which one may obtain the complex absorbing potential (CAP) method by using certain approximations [10]. Although there exists at least three examples in the literature [32–34] which apply the complex scaling method for the computation of vibrational resonances of polyatomic molecules, at present such calculations are mainly carried out [35–39] using the CAP technique. To the best of the authors' knowledge polyatomic rovibrational resonances were only studied within the CAP approach. Therefore, the present study focuses on achievements obtained using CCS. In order to devise a simple methodology and arrive at an efficient code based on the $D^2FOPI$-type protocol, only the 'conventional' complex scaling is considered. The use of alternative complex scaling methods, such as the exterior complex scaling technique, could provide improvements but their consideration is left to the future.

Measuring transitions corresponding to (ro)vibrational resonance states of strongly bound molecules is a complex task; nonetheless, a limited amount of experimental data has been generated. A prime example is the case of the water molecule, where the resonance states have been investigated via state-selective, triple-resonance spectroscopy by Boyarkin *et al.* [40]. The lines in these spectra of water obtained are relatively sparse and have some experimentally determined quantum numbers based on selection rules, which help considerably in their theoretical interpretation. Determination of the complete list of bound vibrational states of water, up to near dissociation, has been the subject of several previous studies [13,41–43]. The global *ab initio* PES of Ref. [13], beyond making it possible to compute nearly all bound states for the system, is fairly accurate even in the asymptotic region. Although it exhibits a dissociation energy some 38 cm$^{-1}$ lower than the experimental value, the vibrational band origins computed with this PES are no more than 15 cm$^{-1}$ off compared to the available experimental results up to 39,500 cm$^{-1}$ above the ZPVE. Thus, this PES is suitable for the computation of

accurate quasi-bound (resonance) states. Therefore, $H_2{}^{16}O$ was chosen as our model molecule. In this sense, this study extends work performed by Zobov *et al*. [44], who employed the PES developed in Ref. [13] and performed computations using the CAP method in order to identify a few measured vibrational and rovibrational Feshbach and shape resonances of the $H_2{}^{16}O$ isotopologue and reported a number of $J = 0$ and 2 and one $J = 1$ resonances for $H_2{}^{16}O$. In a Feshbach resonance the extra energy is temporarily stored in non-dissociative modes (e.g. the symmetric bending and stretching modes in the case of $H_2{}^{16}O$). In a shape resonance the extra life beyond the dissociation limit is provided to the molecule by a rotational barrier and the molecule trapped behind this barrier can escape via quantum mechanical tunneling. Identification of these resonance behaviours is a challenge of non-Hermitian quantum chemistry.

In the forthcoming sections the theoretical methods used are summarised (Section 2), and after a brief overview of the technical details (Section 3) the results on the low-lying (ro)vibrational resonance states of the $H_2{}^{16}O$ water isotopologue are presented along with their comparison to experiment (Section 4). The paper ends with a summary of the results (Section 5).

## 2. Theoretical foundations

### 2.1. *The bound-state (ro)vibrational Hamiltonian*

The Jacobi (also known as scattering) coordinate system [45] and the $R_2$ embedding [46,47] were chosen to set up the rovibrational kinetic energy operator employed in this work. The particularly simple form of this realisation of the triatomic rovibrational Sutcliffe–Tennyson Hamiltonian has been known for a long time [46,47], see, for example, equation (2.12) of Ref. [48]. In this embedding, the $z$-axis of the body-fixed frame is chosen to lie parallel to the atom(O)-diatom($H_2$) vector described by the $R_2$ coordinate. The other two Jacobi-coordinates are the H–H distance ($R_1$), and the angle $\Theta$ between the vectors defining $R_1$ and $R_2$. Use of this coordinate system and embedding makes it possible to exploit a $C_{2v}(M)$ symmetry of the $H_2{}^{16}O$ molecule.

For obtaining the matrix representation of the chosen Hamiltonian an orthogonal, normalised and symmetry-adapted product basis of the form $\{\chi_{n_1}(R_1)\,\chi_{n_2}(R_2)\,P_l^K$ $(\cos\Theta)\,C_{MK}^{Jp}(\phi, \chi, \psi)\}_{n_1=1,n_2=1,K=p,l=K}^{N_1,N_2,J,K+N_L-1}$ was utilised, where $R_1$, $R_2$, and $\Theta$ are the two stretching-type and one bending-type Jacobi coordinates, $\chi_{n_1}(R_1)$ and $\chi_{n_2}(R_2)$ are DVR basis functions, $P_l^K(\cos\Theta)$ is the $\ell$th normalised associated Legendre function, $C_{MK}^{Jp}(\phi, \chi, \psi)$ are rotational functions of the form

$$C_{MK}^{Jp}(\phi, \chi, \psi)$$
$$= [2(1+\delta_{K0})]^{-1/2}\left[D_{MK}^J + (-1)^{p+K+J}\,D_{M-K}^J\right],$$
$$p \in \{0, 1\},\, K \in \{p, p+1, \ldots, J-1, J\},$$

where $p$ is a parity-like variable [49], $M$ and $K$ are the usual quantum numbers corresponding to space- and body-fixed projections of the rotational angular momentum on the appropriate axes, and $D_{MK}^J$ are the normalised Wigner rotation functions [49]. The subsets of basis functions which transform according to the four irreducible representations of the $C_{2v}(M)$ molecular symmetry group are obtained by setting $p = 0$ or 1 and by choosing $\ell + K$ to be odd or even.

Due to the 'almost' direct-product nature of the basis set (almost refers to the coupling between the $P_\ell^K(\cos\Theta)$ Legendre functions and the $C_{MK}^{Jp}(\phi, \chi, \psi)$ rotation functions via $K$ and the parity of $(\ell + K)$, the matrix representation of the triatomic (ro)vibrational Hamiltonian can be written as a sum of direct product matrices.

In order to have a compact basis expansion, $\chi_{n_1}(R_1)$ and $\chi_{n_2}(R_2)$ were chosen to be 'potential optimised' (PO) DVR functions [50–52], i.e. DVR functions obtained from the eigenfunctions of the 1-D effective Hamiltonian $\hat{H}_j^{1D} = -\frac{1}{2\mu_j}\frac{d^2}{dR_j^2} + \hat{V}(R_j; R_{j'}, \Theta), j, j' = 1, 2$ or $2, 1$ with $\hat{V}(R_j; R_{j'}, \Theta)$ chosen to be a relaxed 1-D potential, i.e. $\hat{V}(R_j; R_{j'}, \Theta)$ is obtained by optimising the $R_{j'}$ and $\Theta$ coordinates for each value of $R_j$.

Due to its direct product nature, the matrix representation of the Hamiltonian has a very sparse and *a priori* known structure. This makes the use of an iterative eigensolver, e.g. the Lanczos algorithm [53–55] straightforward for obtaining the required eigenpairs.

### 2.2. *The complex coordinate scaling method*

To compute energies of resonance states, one looks for solutions of the time-independent Schrödinger equation having wavefunctions with exponentially diverging asymptotic behaviour,

$$\hat{H}\Psi^{res} = E^{res}\Psi^{res}, \quad \Psi^{res} \notin L^2. \tag{1}$$

Now, let's introduce an invertible operator $\hat{S}$ to obtain a similarity-transformed Schrödinger equation,

$$\hat{S}\hat{H}\hat{S}^{-1}\hat{S}\Psi^{res} = E^{res}\hat{S}\Psi^{res}, \tag{2}$$

such that the functions $\Phi \equiv \hat{S}\Psi^{res}$ are square integrable, i.e.

$$\hat{S}\hat{H}\hat{S}^{-1}\Phi = E^{res}\Phi,\, \Phi \in L^2. \tag{3}$$

Equation (3) is an eigenvalue equation for the transformed Hamiltonian $\hat{S}\hat{H}\hat{S}^{-1}$, whereby the eigenvalues are the desired resonance eigenenergies and the corresponding eigenfunctions are square integrable; thus, they can be computed with well-developed $L^2$ techniques of quantum chemistry. In the conventional CCS method, a choice for

the operator $\hat{S}$ is

$$\hat{S}_\theta f(r) = f(re^{i\theta}), \qquad (4)$$

where $\theta$ is a free parameter and $r$ is the dissociation coordinate. Therefore, the operator $\hat{S}_\theta$ rotates the argument of a function of the dissociation coordinate by $\theta$ in the complex plane. If there is more than one dissociation coordinate, each should undergo a CCS transformation.

It is well established in the literature [10,24–28] that upon complex scaling by $\hat{S}_\theta$ of Equation (4), (a) only those resonance states will become square integrable for which $\theta > \frac{1}{2}\arctan\left(\Gamma/2\left(\varepsilon - D_0\right)\right) = \frac{1}{2}Arg\left(E^{\mathrm{res}} - D_0\right)$, (b) bound states remain square integrable for $\theta$ values of physical interest, i.e. $\theta < \pi/4$, and (c) the scaled Hamiltonian yields scattering wavefunctions containing combinations of incoming and outgoing waves with bounded, non-square integrable (scattering) asymptotic behaviour which are associated with a continuum that is rotated into the lower half of the complex energy plane by the angle $2\theta$ [24,25,27,28]. Thus, one can come up with a qualitative picture of the spectrum of the scaled Hamiltonian (within the Hilbert-space and the space of bounded, Dirac-normalisable functions), whereby (a) real discrete eigenvalues correspond to bound states, (b) the scattering continuum is rotated into the lower half of the complex plane by $2\theta$ for each dissociation channel, and (c) discrete complex eigenvalues in the area between the real axis and the rotated scattering continua correspond to resonance states.

Obtaining the form of the scaled Hamiltonian is rather straightforward in the case of conventional complex scaling: for differential operators of the dissociation coordinate $r$ one simply needs to make the change $\frac{\partial}{\partial r} \rightarrow \frac{\partial}{\partial r}e^{-i\theta}$, while for the coordinate operators the change $r \rightarrow re^{i\theta}$ is required [24,25]. This naturally leads to the evaluation of the PES at complex coordinate values, which can be done for PESs having a fitted analytical form by rewriting the PES subroutine into complex arithmetic.

During this work, the matrix representation of the scaled Hamiltonian is obtained in two steps. In the first step, all the bound states of the unscaled Hamiltonian are computed, using D²FOPI, along with many eigenpairs having 'energies above the dissociation limit', i.e.

$$\hat{H}\Psi_k = E_k\Psi_k, \quad k \in \{1, 2, \ldots, N\}, \qquad (5)$$

is solved, with $N$ somewhat larger than the number of bound states. In the second step, using a subset of the computed eigenvectors as an orthonormal basis set, the matrix of the scaled Hamiltonian is constructed,

$$\mathbf{H}_{kl}^\theta = \left\langle \Psi_k \right| \hat{S}_\theta \hat{H} \hat{S}_\theta^{-1} \left| \Psi_l \right\rangle, \qquad (6)$$

resulting in a very compact matrix representation. Finally, eigenvalues of the scaled Hamiltonian are obtained via simple direct diagonalisation of the matrix of Equation (6).

Naturally, resonance eigenvalues with a physical meaning should be independent of the scaling parameter $\theta$. However, in practice, when one uses finite basis sets, this is not necessarily true. By changing the scaling parameter, one changes the form of the wavefunctions, thus also changes the 'goodness' of the basis. Therefore, the basis set error and hence the computed eigenvalues depend on the scaling parameter. Nevertheless, it has been demonstrated [56] that resonance eigenvalues can be identified in the CCS formalism by locating stationary points in eigenvalue trajectories obtained by varying the scaling parameter $\theta$. In practice, this can be achieved by computing the spectra of the scaled Hamiltonian for a large number of $\theta$ values and examining the eigenvalue trajectories numerically or visually.

## 3. Computational details

The global PES of $H_2{}^{16}O$ employed is taken from Ref. [13]. This PES is based on high-level electronic structure computations (2200 energy points computed at the all-electron aug-cc-pCV6Z IC-MRCI(8,2) level) and includes relativistic one-electron mass-velocity and Darwin (MVD1) corrections [57]. For all nuclear-motion computations, the nuclear masses $m_O = 15.990526$ u and $m_H = 1.00727647$ u are used.

To ascertain the convergence of the resonance states with respect to basis set size, four sets of 'bound-state' computations (see Equation 5) are performed for $J = 0$. The four sets of computations involve $(n_1, n_2, n_p) = (75,95,50)$, $(85,105,50)$, $(95,115,55)$ and $(100,120,55)$ vibrational basis functions, whereby $(n_1, n_2, n_p)$ means $n_1$ and $n_2$ potential-optimised (PO) spherical-DVR functions [14] (with 400 primitive spherical functions) for the two distance-type coordinates and $n_p$ odd- or even-parity Legendre basis functions for the angle-type coordinate in the case of $B_2$ or $A_1$ symmetry computations, respectively. Following Ref. [14], the spherical oscillator basis functions of the $R_1$ and $R_2$ coordinates had the following parameters: $R_1^{\max} = 19.0$ and $R_2^{\max} = 11.0$ in the first set, $R_1^{\max} = 20.0$ and $R_2^{\max} = 12.0$ in the second set, $R_1^{\max} = 20.5$ and $R_2^{\max} = 12.5$ in the third set, and and $R_1^{\max} = 21.0$ and $R_2^{\max} = 13.0$ in the fourth set (all values are in units of Bohr). The eigenvectors obtained are used for constructing the matrix representation of the CCS $J = 0$ Hamiltonians, see Equation (6). From the four sets, 700, 850, 900 and 992 eigenvectors are taken to construct the Hamiltonian matrices of Equation (6). It is noted that the number of $J = 0$ bound states with $A_1$ and $B_2$ symmetry for $H_2O$ is around 630 and 525, respectively.

For the $J > 0$ computations the (85 105 50) vibrational basis was used with the complete set of rotational basis. In the $J = 1$ case, for constructing the matrices of the CCS Hamiltonians 800 eigenvectors were included for the $A_1$ and $B_2$ symmetry states, while 1400 eigenvectors were included for the $A_2$ and $B_1$ symmetry states. To obtain the eigenvalue trajectories within the CCS method, the scaling parameter $\theta$ was changed between 0.000075 and 0.0030

Table 1. $B_2$-symmetry $J = 0$ Feshbach resonances of the water molecule, obtained from measurement (Expt.) or computation by using the complex coordinate scaling (CCS) technique. Energies and inverse lifetime parameters ($\Gamma$) are given in cm$^{-1}$.

| Expt.[a] | | CCS[b] | | CCS conv.[c] | |
|---|---|---|---|---|---|
| Energy | $\Gamma$ | Energy | $\Gamma$ | Energy | $\Gamma$ |
| 41 172.67(**E**) | 0.21 | 41 175.28 | <0.001[d] | 0.03 | <0.001 |
| 41 203.73(**F**) | 0.22 | 41 205.81 | 0.024 | −0.77 | 0.022 |
| 41 221.23(**H**) | 1 | 41 211.95 | 0.006 | −7.07 | −0.348 |
| 41 225.99(**I**) | 0.42 | 41 225.11 | 0.004 | 0.53 | −0.008 |
| 41 263.56(**K**) | 0.09 | 41 256.31 | 0.364 | −3.18 | −0.312 |
| 41 268.09(**L**) | 0.36 | 41 268.71 | 0.052 | −0.08 | 0.048 |
| 41 295.77(**O**) | 0.52 | 41 288.17 | 0.256 | 0.33 | −0.224 |
| 41 309.76(**B**) | 2.4 | 41 307.10 | 0.156 | −0.34 | −1.12 |

[a] Results are taken from Ref. 44 and they correspond to those reported in Ref. 40. The bold capital letter labels given in parentheses are taken from table 1 of Ref. 44.
[b] Values obtained using the (100 120 55) basis set, see Section 3 for details.
[c] Convergence (conv.) is with respect to results obtained with the (95 115 55) basis set.
[d] The < symbol indicates that the eigenvalue trajectory cusp used to identify the resonance eigenvalue is partly located in the negative $\Gamma$ region of the complex energy plane; thus, $\Gamma$ is only approximated taking into account the size of the region the trajectory samples near the cusp.

Table 2. $J = 0$ Feshbach resonances of the H$_2$$^{16}$O molecule, computed with either the complex absorbing potential (CAP) or the complex coordinate scaling (CCS) resonance determining methods. Energies and inverse lifetime parameters ($\Gamma$) are given in cm$^{-1}$.

| $B_2$ symmetry | | | | | | $A_1$ symmetry | | | |
|---|---|---|---|---|---|---|---|---|---|
| CAP[a] | | CCS[b] | | CCS conv.[c] | | CCS[d] | | CCS conv.[e] | |
| Energy | $\Gamma$ | Energy | $\Gamma$ | Energy | $\Gamma$ | Energy | $\Gamma$ | Energy | $\Gamma$ |
| – | – | 41111.12 | <0.001[f] | −0.08 | <0.001 | 41109.90 | 0.0045 | −0.23 | −0.0021 |
| 41119.69 | 0.01 | 41113.59 | <0.001 | 0.03 | <0.001 | 41133.57 | 0.048 | −0.43 | −0.018 |
| – | – | 41137.73 | <0.001 | – | – | 41168.15 | 0.0095 | −0.15 | 0.0049 |
| 41140.49 | 2.03 | – | – | – | – | 41212.13 | 0.018 | – | – |
| 41175.29 | 0.002 | 41175.28 | <0.001 | −0.03 | <0.001 | 41214.44 | 0.020 | – | – |
| 41206.29 | 0.33 | 41205.81 | 0.024 | −0.77 | 0.022 | 41247.00 | 0.0071 | – | – |
| – | – | 41211.95 | 0.006 | −7.07 | −0.348 | 41259.42 | 0.185 | −0.17 | −0.037 |
| 41224.39 | 0.3 | 41225.11 | 0.004 | 0.53 | −0.008 | 41277.35 | 0.125 | 0.87 | −0.013 |
| 41257.79 | 0.03 | 41256.31 | 0.364 | −3.18 | −0.312 | 41286.30 | 0.13 | 1.84 | 0.14 |
| 41268.99 | 0.12 | 41268.71 | 0.052 | −0.08 | 0.048 | | | | |
| 41275.09 | 20.14 | – | – | – | – | | | | |
| – | – | 41288.17 | 0.256 | 0.33 | −0.224 | | | | |
| – | – | 41307.10 | 0.156 | −0.34 | –1.12 | | | | |

[a] Results taken from Ref. [44].
[b] Values were obtained using the (100 120 55) basis set, see Section 3 for details.
[c] Convergence is with respect to results obtained with the (95 115 55) basis set, missing convergence values indicate that those resonances were only identified using the largest (100 120 55) basis set.
[d] Values were obtained using the (85 105 50) basis set, see Section 3 for details.
[e] Convergence is with respect to results obtained with the (75 95 50) basis set, missing convergence values indicate that those resonances were only identified using the (85 105 50) basis set.
[f] The < symbol indicates that the eigenvalue trajectory cusp used to identify the resonance eigenvalue is partly located in the negative $\Gamma$ region of the complex energy plane; thus, $\Gamma$ is only approximated taking into account the size of the region the trajectory samples near the cusp.

in thirteen steps and the resonance cusps were identified by visual inspection.

## 4. Results and discussion

Table 1 lists computed $B_2$-symmetry $J = 0$ Feshbach resonance energies and inverse lifetime parameters $\Gamma$ obtained in this study, along with their experimental counterparts [40] up to about 210 cm$^{-1}$ above the dissociation limit.

Although theoretical results are available for much higher energies as well, this energy range is considered throughout this work. Table 2 provides computed $J = 0$ Feshbach resonances of this study and their comparison with previous theoretical results obtained with the CAP method. A list of $J = 1$ rovibrational resonances computed as part of this study are presented in Table 3. Two-dimensional sections of the computed $|\hat{S}_\theta \Psi^{\text{res}}|^2$ probability density functions are provided on Figures 1–8 and 9–19 for $J = 0$ and 1 states,

Table 3. $J = 1$ rovibrational resonances of the H$_2{}^{16}$O molecule, computed with the complex coordinate scaling (CCS)[a] method. Energies and inverse lifetime parameters ($\Gamma$) are given in cm$^{-1}$.

| $A_1$ symmetry | | $A_2$ symmetry | | $B_1$ symmetry | | $B_2$ symmetry | |
|---|---|---|---|---|---|---|---|
| Energy | $\Gamma$ | Energy | $\Gamma$ | Energy | $\Gamma$ | Energy | $\Gamma$ |
| 41144.52 | 2.04E-01 | 41117.14 | <3.00E-03[b] | 41108.30 | 1.70E-03 | 41128.00 | 6.00E-04 |
| 41145.74 | 7.60E-01 | 41117.58 | <5.00E-03 | 41117.15 | <3.00E-03 | 41132.52 | 5.36E-02 |
| 41155.84 | 1.29E-03 | 41124.44 | <3.00E-03 | 41124.45 | <3.00E-03 | 41139.95 | 1.85E-02 |
| 41163.73 | 9.70E-04 | 41129.36 | 9.64E-03 | 41129.73 | 4.98E-03 | 41144.92 | 4.56E-02 |
| 41174.18 | 1.83E-02 | 41135.05 | 9.02E-03 | 41132.96 | 2.90E-02 | 41158.50 | 2.52E-02 |
| 41210.69 | 9.07E-04 | 41136.44 | 4.78E-02 | 41135.06 | 3.08E-02 | 41166.13 | 6.62E-02 |
| 41213.39 | 8.08E-03 | 41142.07 | 2.60E-02 | 41137.07 | <6.00E-03 | 41184.50 | 7.10E-03 |
| 41223.65 | 3.86E-05 | 41145.27 | 1.32E-02 | 41137.88 | 5.98E-01 | 41191.05 | 8.30E-02 |
| 41246.56 | 1.69E-02 | 41146.16 | 2.64E-01 | 41141.70 | 3.14E-02 | 41210.72 | 2.28E-03 |
| 41304.73 | 8.33E-05 | 41150.29 | 2.04E-01 | 41145.65 | 3.34E-03 | 41214.06 | 4.58E-03 |
| 41315.32 | 7.12E-01 | 41162.85 | 1.61E-01 | 41146.17 | 1.16E-01 | 41247.96 | 2.18E-02 |
| | | 41170.38 | 2.18E-01 | 41150.60 | 2.52E-02 | 41298.60 | 2.38E-04 |
| | | 41178.35 | 1.87E-02 | 41166.63 | 2.50E-01 | | |
| | | 41191.67 | 1.87E-01 | 41186.47 | 1.77E-01 | | |
| | | 41199.61 | 3.70E-02 | 41193.16 | <4.00E-03 | | |
| | | 41194.54 | <2.00E-03 | 41199.86 | 3.20E-02 | | |
| | | 41211.66 | 2.62E-01 | 41212.05 | 1.53E-01 | | |
| | | 41214.50 | 5.60E-02 | 41215.08 | 1.18E-02 | | |
| | | 41222.96 | 1.20E-01 | 41234.93 | 3.80E-01 | | |
| | | 41224.61 | 3.22E-01 | 41241.29 | <4.00E-05 | | |
| | | 41272.60 | 1.03E-01 | 41272.26 | 2.88E-01 | | |
| | | 41280.15 | 8.28E-01 | 41278.32 | 8.22E-02 | | |
| | | 41283.52 | 1.49E-01 | 41290.61 | 5.38E-01 | | |
| | | 41290.73 | 2.24E-01 | 41295.63 | 1.45E-02 | | |
| | | 41297.80 | 5.56E-01 | 41298.22 | <1.00E-03 | | |
| | | 41307.37 | 4.02E-01 | | | | |

[a]Values were obtained using the (85 105 50) basis set, see Section 3 for details.
[b]The < symbol indicates that the eigenvalue trajectory cusp used to identify the resonance eigenvalue is partly located in the negative $\Gamma$ region of the complex energy plane; thus, $\Gamma$ is only approximated taking into account the size of the region the trajectory samples near the cusp.

respectively. These figures, corresponding to $B_2$ and $A_1$ symmetry for $J = 0$ and 1, respectively, are presented in order of increasing energy. For the $J = 1$ cases, integration along the rotational coordinates was carried out prior to drawing the figures.

### 4.1. Vibrational ($J = 0$) resonances

In order to test our algorithms and codes, developed during this study based on the CCS method described in Section 2.2, the CAP-based $J = 0$ nuclear motion results of Zobov *et al.* [44] are used as benchmark values. This
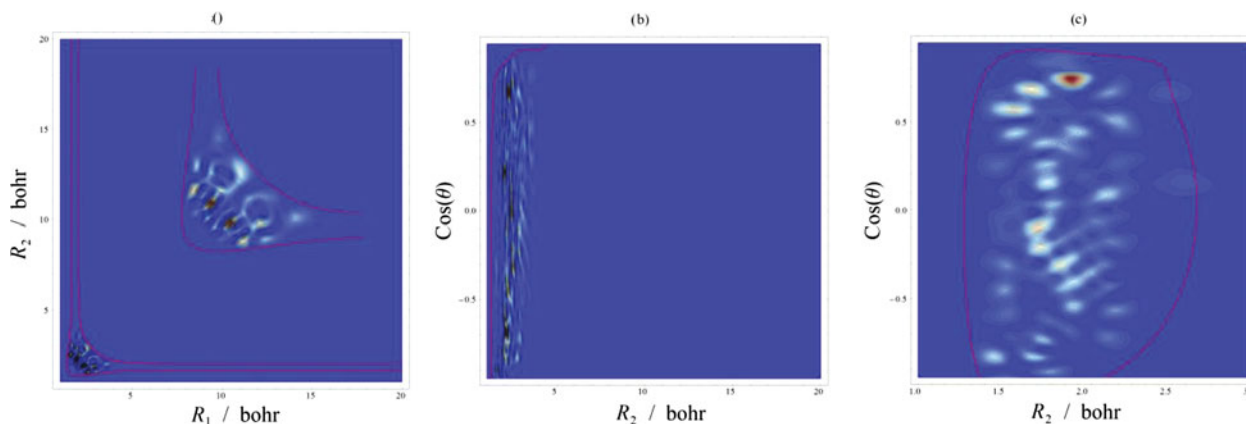


Figure 1. Two-dimensional sections of the wavefunction corresponding to the $J = 0$ resonance at 41,111 cm$^{-1}$ with $\Gamma = 0.0001$ cm$^{-1}$, obtained by fixing (a) $\mathrm{Cos}(\theta) = 0.65$, (b) $R_1 = 1.9$ Bohr, and (c) $R_1 = 2.8$ Bohr, where $R_1$ and $R_2$ are the two OH bond lengths and $\theta$ is the HOH bond angle. The area near the equilibrium structure is shown enlarged in (a).
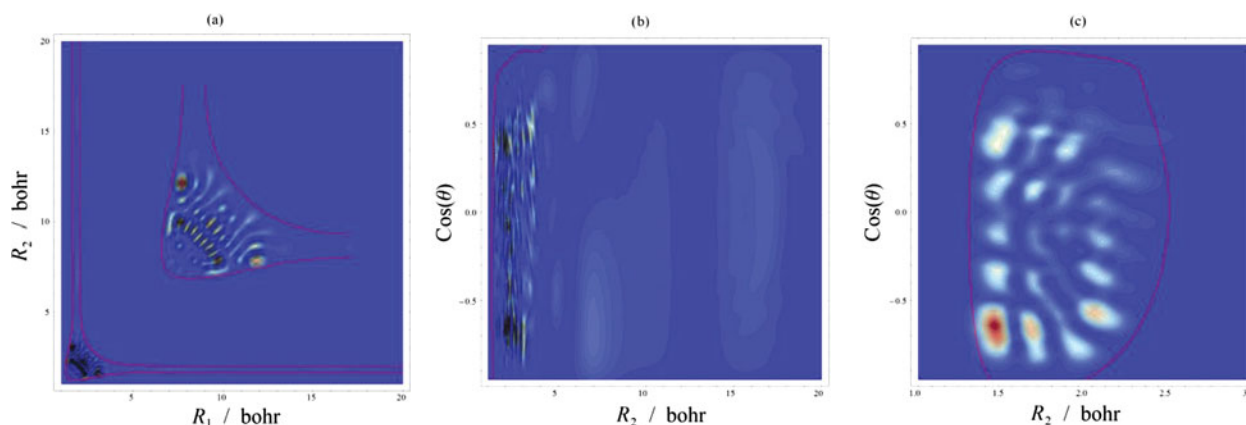
Figure 2.　Two-dimensional sections of the wavefunction corresponding to the $J = 0$ resonance at 41,114 cm$^{-1}$ with $\Gamma = 0.002$ cm$^{-1}$, obtained by fixing (a) $\cos(\theta) = -0.65$, (b) $R_1 = 1.9$ Bohr, and (c) $R_1 = 3.0$ Bohr, where $R_1$ and $R_2$ are the two OH bond lengths and $\theta$ is the HOH bond angle. The area near the equilibrium structure is shown enlarged in (a).
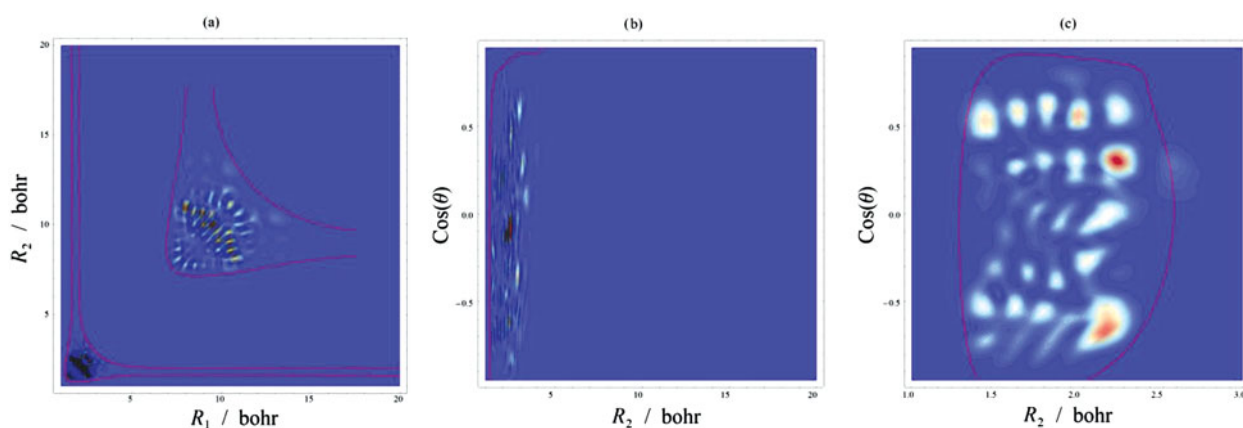


Figure 3.　Two-dimensional sections of the wavefunction corresponding to the $J = 0$ resonance at 41,175 cm$^{-1}$ with $\Gamma = 0.00015$ cm$^{-1}$, obtained by fixing (a) $\cos(\theta) = -0.1$, (b) $R_1 = 1.9$ Bohr, and (c) $R_1 = 2.9$ Bohr, where $R_1$ and $R_2$ are the two OH bond lengths and $\theta$ is the HOH bond angle. The area near the equilibrium structure is shown enlarged in a).
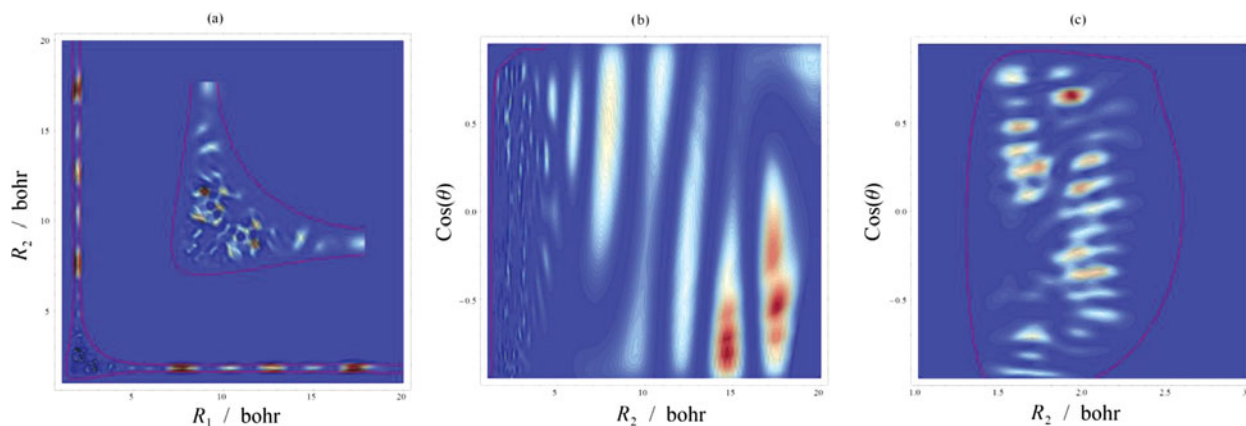


Figure 4.　Two-dimensional sections of the wavefunction corresponding to the $J = 0$ resonance at 41,202 cm$^{-1}$ with $\Gamma = 0.244$ cm$^{-1}$, obtained by fixing (a) $\cos(\theta) = 0.1$, (b) $R_1 = 1.9$ Bohr, and (c) $R_1 = 2.9$ Bohr, where $R_1$ and $R_2$ are the two OH bond lengths and $\theta$ is the HOH bond angle. The area near the equilibrium structure is shown enlarged in (a).
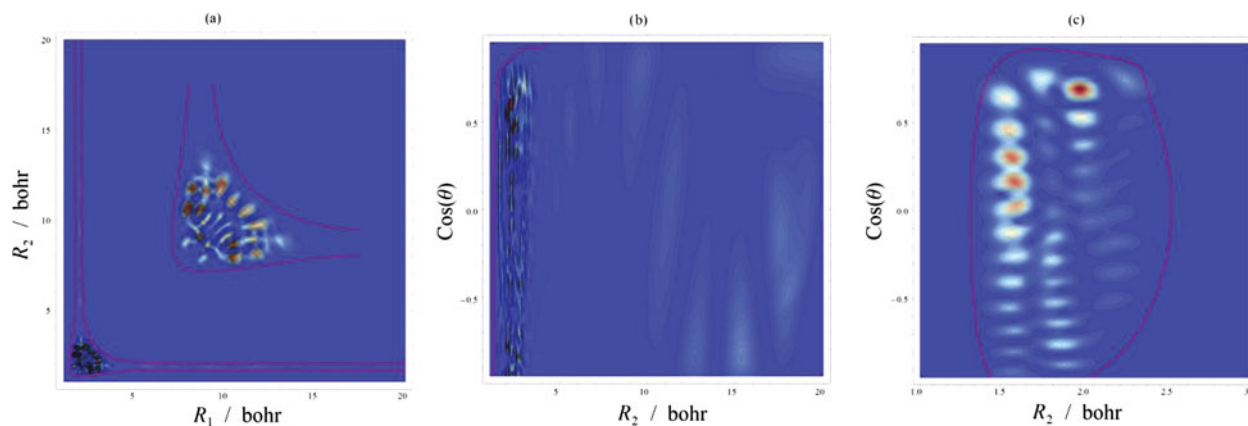
Figure 5. Two-dimensional sections of the wavefunction corresponding to the $J = 0$ resonance at 41,225 cm$^{-1}$ with $\Gamma = 0.032$ cm$^{-1}$, obtained by fixing (a) $\mathrm{Cos}(\theta) = 0.5$, (b) $R_1 = 1.9$ Bohr, and (c) $R_1 = 3.0$ Bohr, where $R_1$ and $R_2$ are the two OH bond lengths and $\theta$ is the HOH bond angle. The area near the equilibrium structure is shown enlarged in (a).
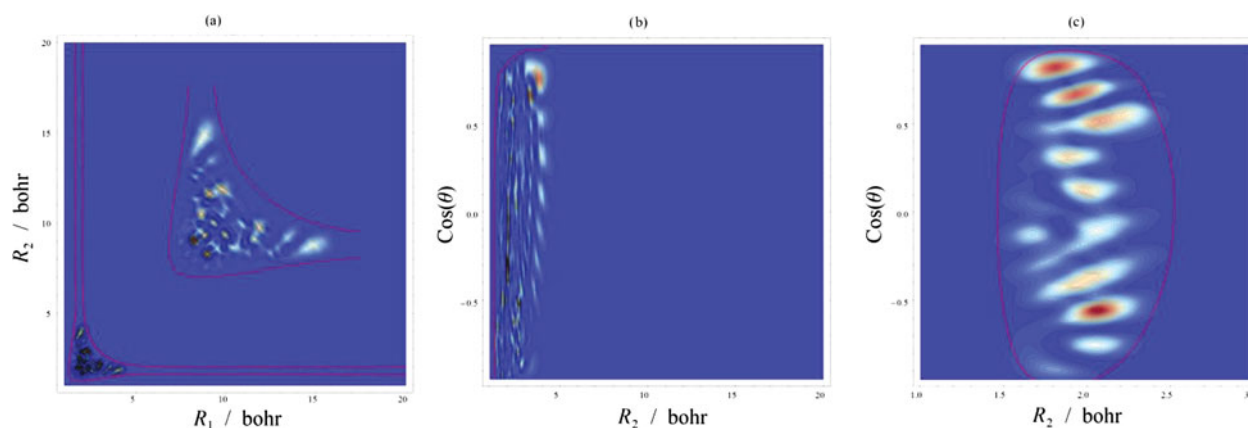


Figure 6. Two-dimensional sections of the wavefunction corresponding to the $J = 0$ resonance at 41,258 cm$^{-1}$ with $\Gamma = 0.002$ cm$^{-1}$, obtained by fixing (a) $\mathrm{Cos}(\theta) = 0.1$, (b) $R_1 = 1.9$ Bohr, and (c) $R_1 = 3.5$ Bohr, where $R_1$ and $R_2$ are the two OH bond lengths and $\theta$ is the HOH bond angle. The area near the equilibrium structure is shown enlarged in (a).
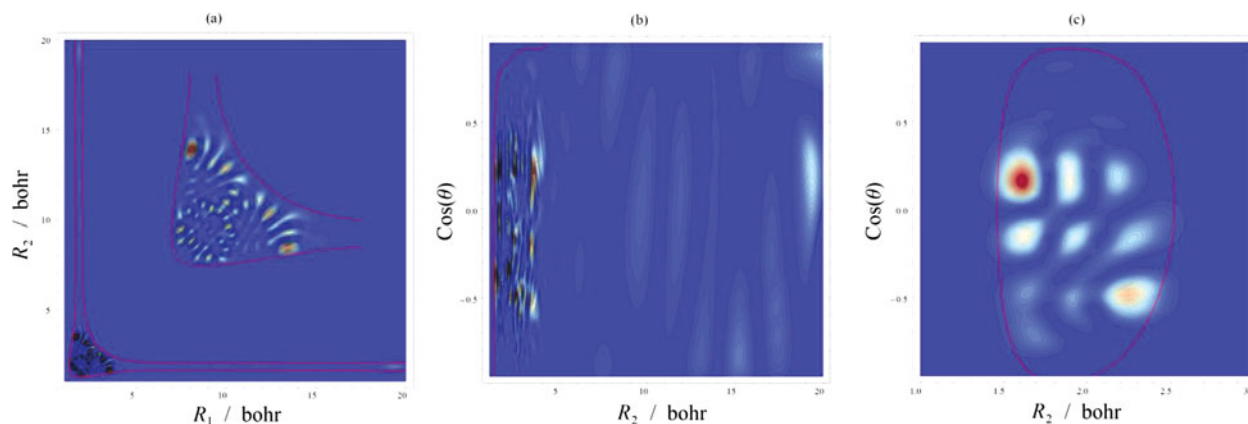


Figure 7. Two-dimensional sections of the wavefunction corresponding to the $J = 0$ resonance at 41,269 cm$^{-1}$ with $\Gamma = 0.095$ cm$^{-1}$, obtained by fixing (a) $\mathrm{Cos}(\theta) = 0.2$, (b) $R_1 = 1.9$ Bohr, and (c) $R_1 = 3.5$ Bohr, where $R_1$ and $R_2$ are the two OH bond lengths and $\theta$ is the HOH bond angle. The area near the equilibrium structure is shown enlarged in (a).
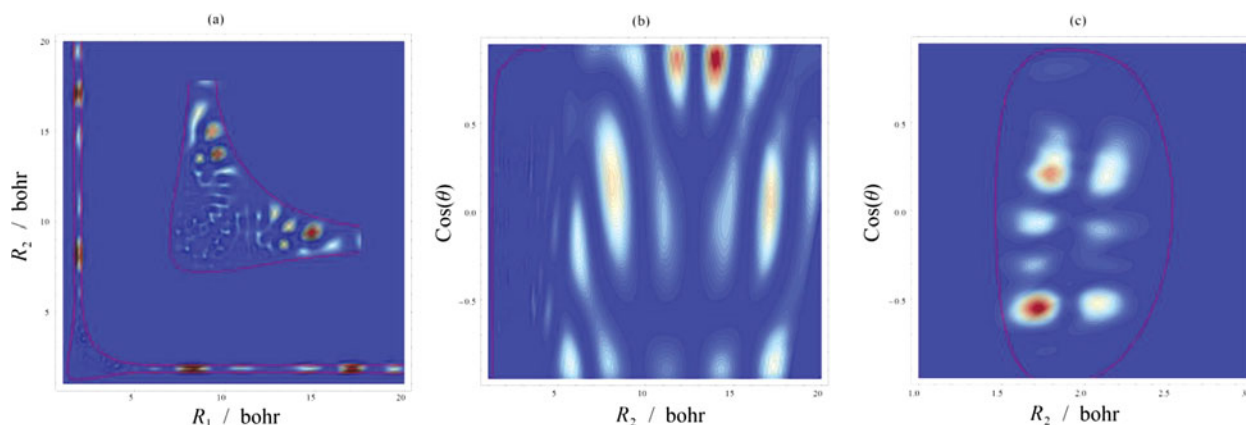
Figure 8. Two-dimensional sections of the wavefunction corresponding to the $J = 0$ resonance at 41,286 cm$^{-1}$ with $\Gamma = 0.572$ cm$^{-1}$, obtained by fixing (a) $\text{Cos}(\theta) = 0.1$, (b) $R_1 = 1.9$ Bohr, and (c) $R_1 = 3.5$ Bohr, where $R_1$ and $R_2$ are the two OH bond lengths and $\theta$ is the HOH bond angle. The area near the equilibrium structure is shown enlarged in (a).

comparison is feasible as both computations utilise the same global PES of $H_2{}^{16}O$ [13].

When comparing their computed resonance energies with experiment, Zobov *et al.* [44] shifted theoretical energy values above the first dissociation limit by 38 cm$^{-1}$, to account for the following weakness of the PES: it exhibits a dissociation energy of $D_0 = 41,108$ cm$^{-1}$, which is 38 cm$^{-1}$ lower than the experimental value [58] of $41,145.94 \pm 0.15$ cm$^{-1}$. Resonance wavefunctions, although damped by the CAP, were considered to have a structure similar to the bound-state wavefunctions with energies just below dissociation, i.e. they were considered to be localised in the asymptotic region of the PES. Although some features of the experimental spectra were reconstructed, energy differences often reached a few tens of cm$^{-1}$ for several of the features **A** through **R** discussed there.

In Table 1 of this study vibrational Feshbach resonances computed as part of this work of the most abundant water isotopologue are presented. Experimental values and their assignment are taken from Refs. [40,44], while theoretical values computed with complex scaling, and their convergence with respect to basis set size, are from this work. Assignment of the results from complex scaling was done by simply matching energies with experimental values. It is remarkable that the resonance energies obtained with complex scaling reproduce the experimental values with considerable accuracy, despite the fact that no energy shifting is applied.

Comparison of the theoretical results obtained with the CAP method and without shifting the energies is summarised in Table 2. As far as the energy values are concerned the computations show good agreement with experiment. The inverse lifetime parameter $\Gamma$ seems to converge much more slowly than the energy; therefore, lifetimes are not taken into account when matching the computed eigenvalues obtained via the CAP and CCS techniques. It is important to point out that there are resonance states, which are obtained with only one of the computational methods. It is not surprising to have some results only determined with the CCS method, since the CAP method is not guaranteed to identify 'all' resonance states, as already seen, for example, in Ref. [32]. As to eigenvalues computed only by the CAP method, they have large $\Gamma$ parameters (thus, short lifetimes), so they remain 'hidden' in the range of $\theta$ used in the CCS computations.

Based on Tables 1 and 2, one may conclude that the energy shifting used in Ref. [44] was unnecessary for the $J = 0$ Feshbach resonances; therefore, the present work suggests changes in the previous assignments.

A possible qualitative explanation for why the computed $J = 0$ Feshbach resonances do not need the energy shifting may lie in the very nature of this type of resonance. Feshbach resonances arise when the system has enough energy to dissociate; however, a considerable amount of energy is localised in non-dissociative vibrational modes. If for a given Feshbach resonance state of water a significant portion of the energy is stored in non-dissociative modes, such as the bending or the symmetric streching modes, this leads to less energy in the dissociative stretching mode, which in turn means that the wave function is less delocalised in the dissociative coordinate. Therefore, the inaccuracies in the PES which are responsible for the discrepancy in the dissociation energy, and which are restricted to the asymptotic regions of the stretching coordinates, are not sampled dominantly by Feshbach resonance states. This qualitative explanation can be justified at least for some of the resonances by inspecting the appropriate $J = 0$ probability density plots. These plots are discussed separately in Section 4.3, in particular Figures 1, 3, 5–7 are relevant for supporting the argument presented.

### 4.2. Rovibrational, J = 1, resonances

Computation of rovibrational resonance eigenpairs and their comparison with vibrational resonances can lead to interesting observations about the question whether a computed resonance is of Feshbach or of shape type or perhaps a mixture of the two and what effect rotation has on Feshbach resonances. Altogether 74 $J = 1$ resonances were identified up to around 210 cm$^{-1}$ above $D_0$, which is somewhat more than three times the number of $J = 0$ resonances found in this energy region. This indicates that even for the low rotational quantum number of $J = 1$, formation of shape resonances seems to occur. Discussion of these resonances is postponed to Section 4.3. Sorting the shape resonances could not be achieved in this study. Therefore, possible tunneling effects are not investigated.

### 4.3. Plots of resonance states

In this subsection selected plots of probability densities (Figures 1–19), obtained from the computed eigenfunctions (using the (85 105 50) basis) corresponding to resonance eigenvalues, are presented and discussed. It is noted that although the underlying computations were carried out in Jacobi coordinates, the eigenfunctions on Figures 1–19 are presented as functions of the internal OH stretch and HOH bend angle coordinates in order to have figures whose interpretation is more natural and intuitive. It is important to emphasise that the functions obtained from CCS resonance computations are not the $\Psi^{res}$ resonance wavefunctions but the CCS wavefunctions, i.e. $\hat{S}_\theta \Psi^{res}$. Therefore, one needs to examine the physical significance of the probability density functions $|\hat{S}_\theta \Psi^{res}|^2$. A possible route is the inspection of the probability density functions of bound states, which can be obtained both with and without the use of CCS. Comparison of the $|\hat{S}_\theta \Psi^{bound}|^2$ and $|\Psi^{bound}|^2$ functions of three bound states with excitation energies 11,032, 39,511, and 41,046 cm$^{-1}$ clearly show (not detailed here) that, as expected, CCS does not change the probability density visibly in the non-asymptotic coordinate regions, i.e. up to OH lengths of 10 Bohr no change is visible. Therefore, interpretation of the CCS probability densities of resonance states might be done in a similar manner as usually done for bound states.

Although strictly speaking there are no distinct vibrational modes for a non-harmonic coupled system and one would expect extreme vibrational coupling at the high energies of the resonance states, a great deal of qualitative information can be gathered from the probability density plots generated. Clearly, detailed inspection of the density functions reveals much about the intrinsic nature of the low-lying rovibrational resonance states of $H_2^{16}O$. There are several questions which probability density plots should help to answer: (1) Which non-dissociative vibrational modes are highly excited during formation of

Feshbach resonances (it has been argued [44] that resonance states with $(m,0)^\pm v_2$ in local mode notation with $v_2$ = 0, 1 or 2 should be the observable ones as below dissociation these states are the ones most easily observed and they have [44] the strongest dipole transitions)? (2) How regular are the resonance states (it has been argued before [59,60] that 'chaotic' resonance states couple strongly to the continuum and thus have no significant lifetimes)? (3) Can one distinguish between Feshbach and shape resonances at the low $J = 1$ rotational excitation investigated here? (4) What effect does the inclusion of rotation have on Feshbach resonances?

The $J = 0$ plot of Figure 7 shows nine nodes along the antisymmetric stretching coordinate and around three nodes along the symmetric stretch, while only two bending nodes are present. This low level of bending excitation is the expected behaviour for resonance states. While the $J = 0$ states of Figures 4 and 8 have high excitation in their stretching modes, Figures 2 and 5 demonstrate a pattern of symmetric and antisymmetric stretches similar to Figure 7.

The $J = 0$ states of Figures 4 and 5 show a completely different resonance behaviour, as these states contain at least 10 nodes along the bending motion. This is an unexpected result of the present study.

By further inspecting Figures 1, 3, 5–7, it seems that for $H_2^{16}O$ purely vibrational ($J = 0$) Feshbach resonances can be formed via the accumulation of the energy in either the bending, the symmetric streching, or the antisymmetric streching modes. Naturally, dissociation must occur along the stretching of an OH bond, while the other OH bond is fixed approximately between 1.7 and 2.0 Bohrs. This is represented by the correlation between the shortening of the state lifetime (increase in $\Gamma$) with respect to the excitation of the stretching motion.

Wavefunction plots should also provide insight into the state-specific dissociation dynamics of the water molecule. For example, in panels (b) of Figures 4, 5 and 7 one can see a horse-shoe type feature in the density function, indicating that dissociation occurs by first closing and then opening of the HOH bond angle as one of the H atoms leaves the molecule. The opposite route of closing the HOH angle as one of the H atoms dissociates can be observed in panel (b) of Figure 19, while panels (b) of Figures 9, 10, 13–15 show more or less constant HOH bond angles at which dissociation can occur, resulting in the H atom leaving the molecule either perpendicular (Figures 9, 10 and 13) or parallel to the OH diatom bond.

An interesting feature of the plots is the remarkable similarity between the rovibrational ($J = 1$) and the vibrational ($J = 0$) resonance density functions when comparing Figures 7 and 18 as well as Figures 3 and 16. Clearly, one can relate the rovibrational resonance states of Figures 16 and 18 to the vibrational resonance states of Figures 3 and 7, respectively. The increase in energy with the inclusion of rotation is 49 and 36 cm$^{-1}$ for the vibrational states at
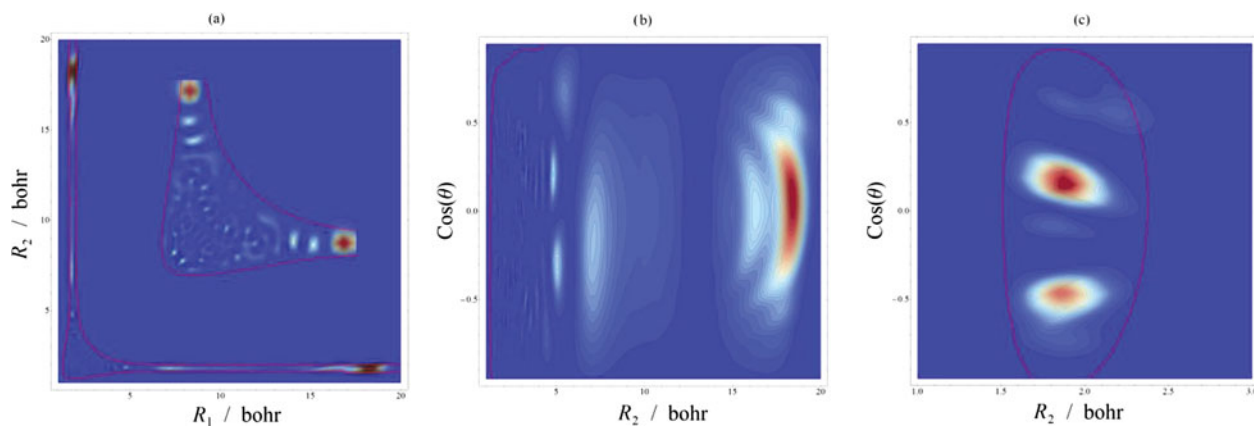
Figure 9. Two-dimensional sections of the wavefunction corresponding to the $J = 1$ resonance at 41,145 cm$^{-1}$ with $\Gamma = 0.204$ cm$^{-1}$, obtained by fixing (a) Cos($\theta$) = 0.1, (b) $R_1 = 2.0$ Bohr, and (c) $R_1 = 3.8$ Bohr, where $R_1$ and $R_2$ are the two OH bond lengths and $\theta$ is the HOH bond angle. The area near the equilibrium structure is shown enlarged in (a).
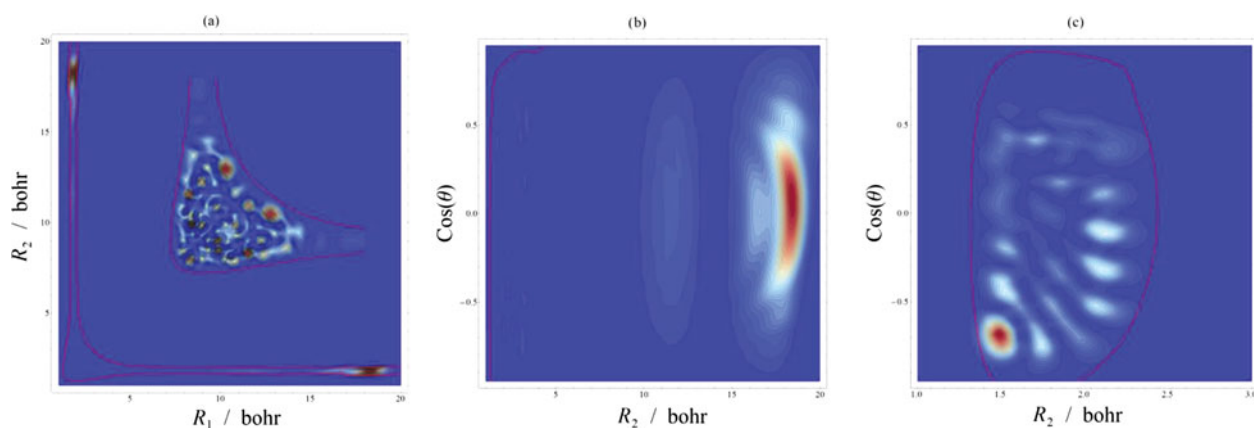


Figure 10. Two-dimensional sections of the wavefunction corresponding to the $J = 1$ resonance at 41,146 cm$^{-1}$ with $\Gamma = 0.76$ cm$^{-1}$, obtained by fixing (a) Cos($\theta$) = 0.1, (b) $R_1 = 1.9$ Bohr, and (c) $R_1 = 3.1$ Bohr, where $R_1$ and $R_2$ are the two OH bond lengths and $\theta$ is the HOH bond angle. The area near the equilibrium structure is also shown enlarged in (a).
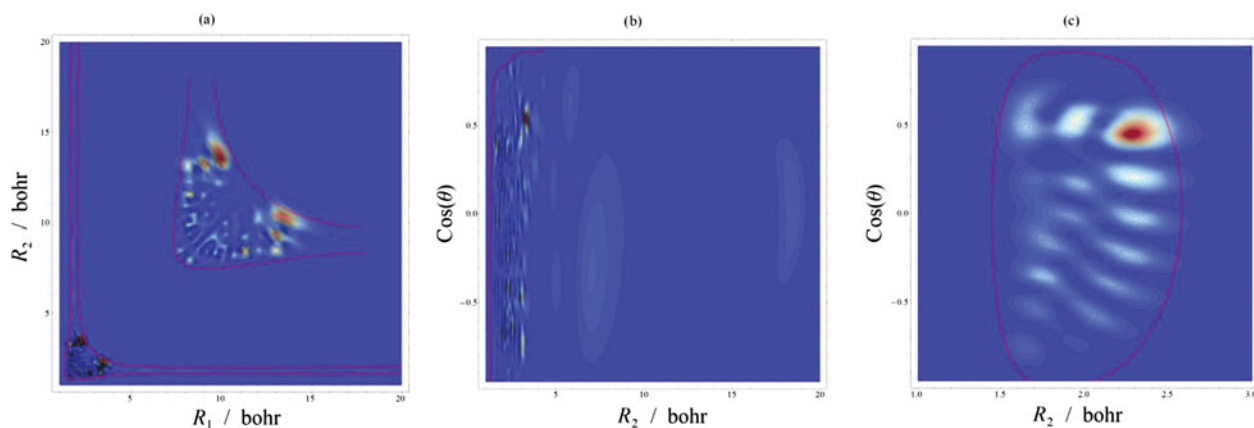


Figure 11. Two-dimensional sections of the wavefunction corresponding to the $J = 1$ resonance at 41,156 cm$^{-1}$ with $\Gamma = 0.0013$ cm$^{-1}$, obtained by fixing (a) Cos($\theta$) = 0.5, (b) $R_1 = 1.9$ Bohr, and (c) $R_1 = 3.4$ Bohr, where $R_1$ and $R_2$ are the two OH bond lengths and $\theta$ is the HOH bond angle. The area near the equilibrium structure is shown enlarged in (a).
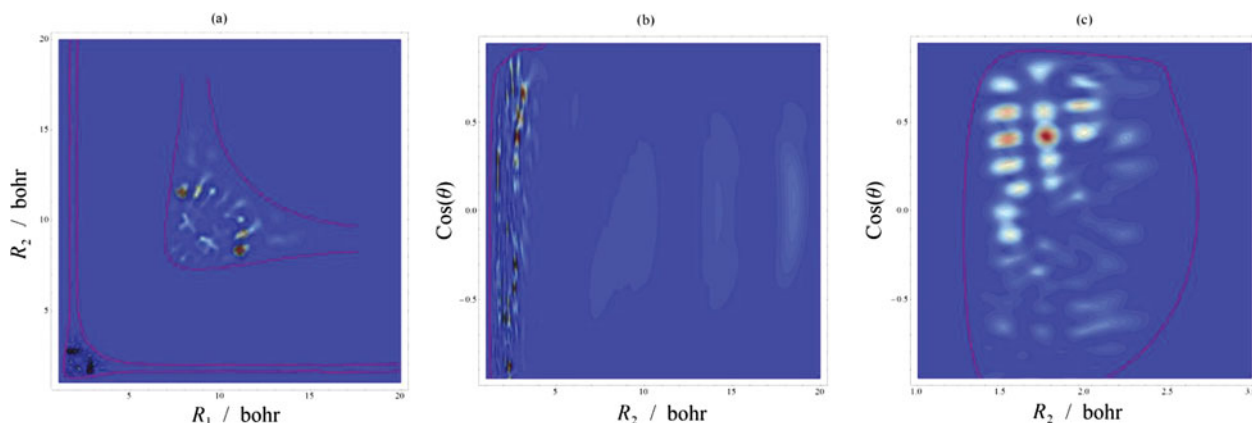
Figure 12.   Two-dimensional sections of the wavefunction corresponding to the $J = 1$ resonance at 41,164 cm$^{-1}$ with $\Gamma = 0.0010$, obtained by fixing (a) $\text{Cos}(\theta) = 0.4$, (b) $R_1 = 1.9$ Bohr, and (c) $R_1 = 2.8$ Bohr, where $R_1$ and $R_2$ are the two OH bond lengths and $\theta$ is the HOH bond angle. The area near the equilibrium structure is shown enlarged in (a).
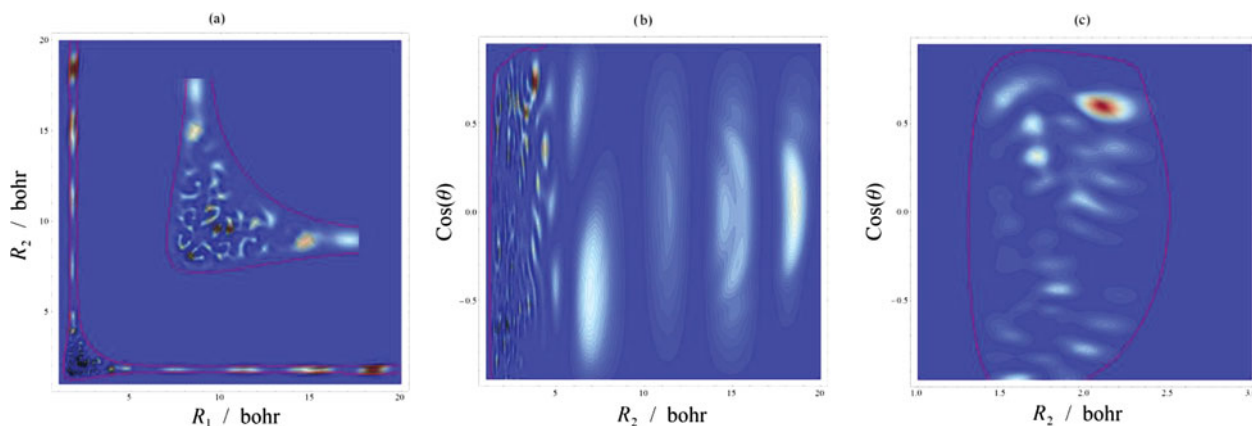


Figure 13.   Two-dimensional sections of the wavefunction corresponding to the $J = 1$ resonance at 41,174 cm$^{-1}$ with $\Gamma = 0.018$ cm$^{-1}$, obtained by fixing (a) $\text{Cos}(\theta) = 0.1$, (b) $R_1 = 1.9$ Bohr, and (c) $R_1 = 3.0$ Bohr, where $R_1$ and $R_2$ are the two OH bond lengths and $\theta$ is the HOH bond angle. The area near the equilibrium structure is shown enlarged in (a).
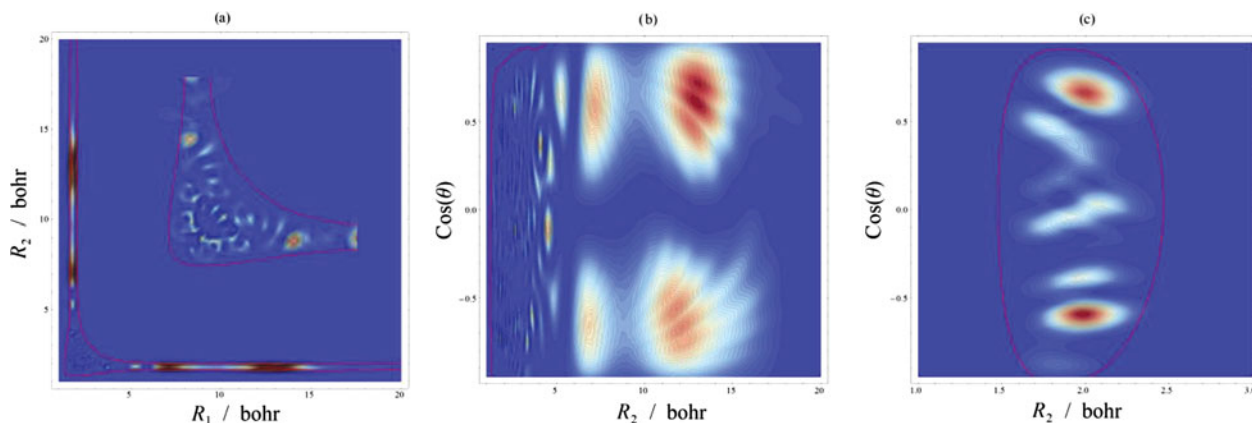


Figure 14.   Two-dimensional sections of the wavefunction corresponding to the $J = 1$ resonance at 41,211 cm$^{-1}$ with $\Gamma = 0.0009$ cm$^{-1}$, obtained by fixing (a) $\text{Cos}(\theta) = 0.5$, (b) $R_1 = 1.9$ Bohr, and (c) $R_1 = 3.6$ Bohr, where $R_1$ and $R_2$ are the two OH bond lengths and $\theta$ is the HOH bond angle. The area near the equilibrium structure is shown enlarged in (a).
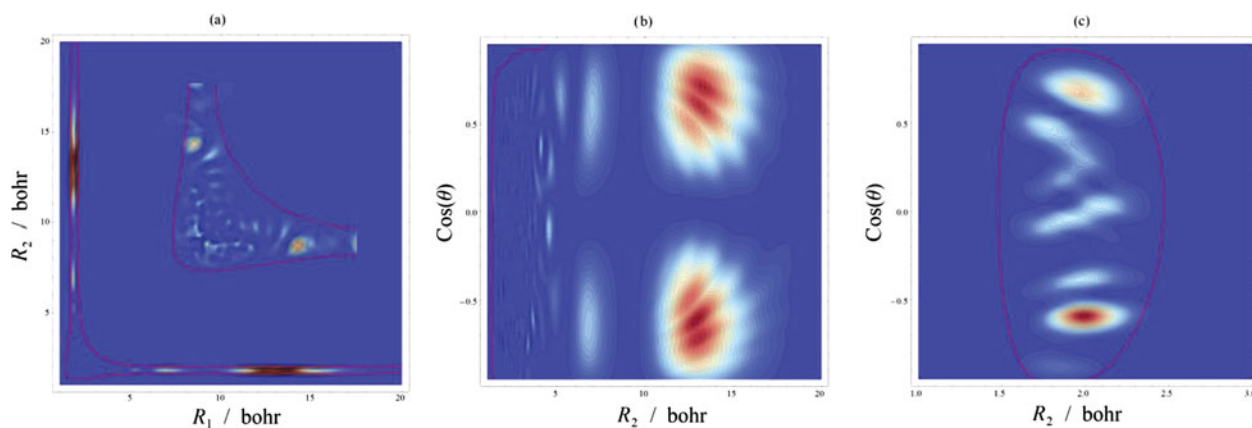
Figure 15. Two-dimensional sections of the wavefunction corresponding to the $J = 1$ resonance at 41,213 cm$^{-1}$ with $\Gamma = 0.0081$ cm$^{-1}$, obtained by fixing (a) Cos($\theta$) = 0.5, (b) $R_1 = 1.9$ Bohr, and (c) $R_1 = 3.6$ Bohr, where $R_1$ and $R_2$ are the two OH bond lengths and $\theta$ is the HOH bond angle. The area near the equilibrium structure is shown enlarged in (a).
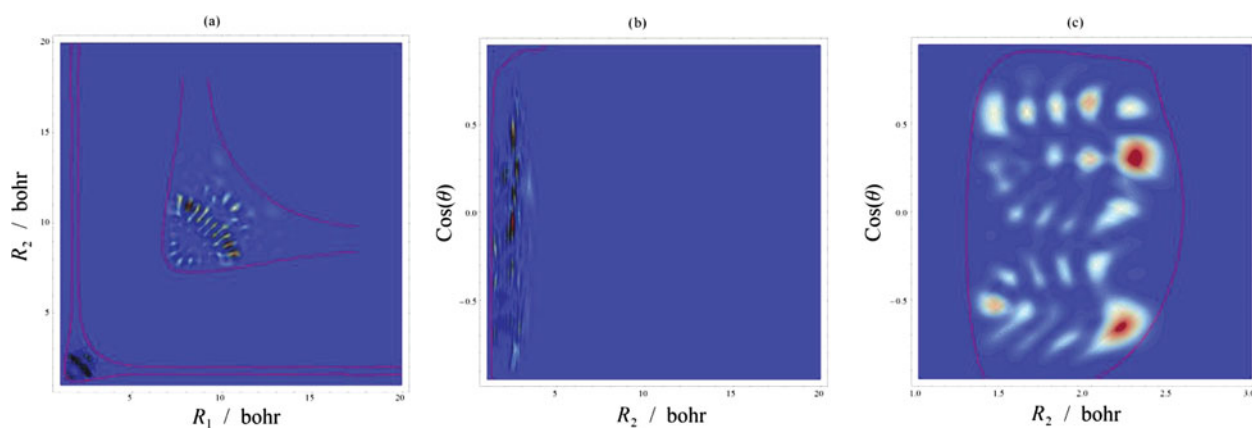


Figure 16. Two-dimensional sections of the wavefunction corresponding to the $J = 1$ resonance at 41,224 cm$^{-1}$ with $\Gamma = 0.00004$, obtained by fixing (a) Cos($\theta$) = $-0.1$, (b) $R_1 = 1.9$ Bohr, and (c) $R_1 = 2.9$ Bohr, where $R_1$ and $R_2$ are the two OH bond lengths and $\theta$ is the HOH bond angle. The area near the equilibrium structure is shown enlarged in (a).
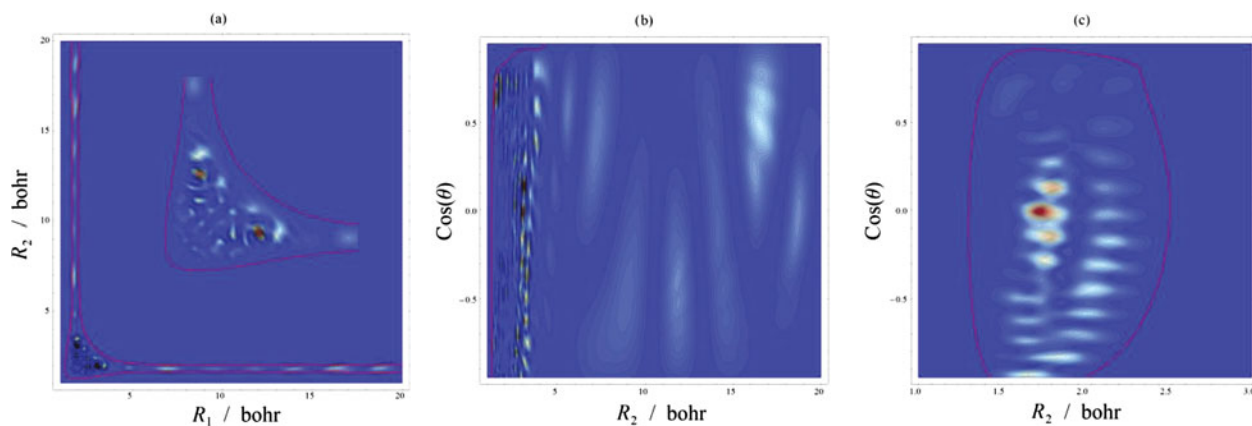


Figure 17. Two dimensional sections of the wavefunction corresponding to the $J = 1$ resonance at 41,247 cm$^{-1}$ with $\Gamma = 0.017$ cm$^{-1}$, obtained by fixing (a) Cos($\theta$) = 0.1, (b) $R_1 = 1.9$ Bohr, and (c) $R_1 = 3.0$ Bohr, where $R_1$ and $R_2$ are the two OH bond lengths and $\theta$ is the HOH bond angle. The area near the equilibrium structure is shown enlarged in (a).
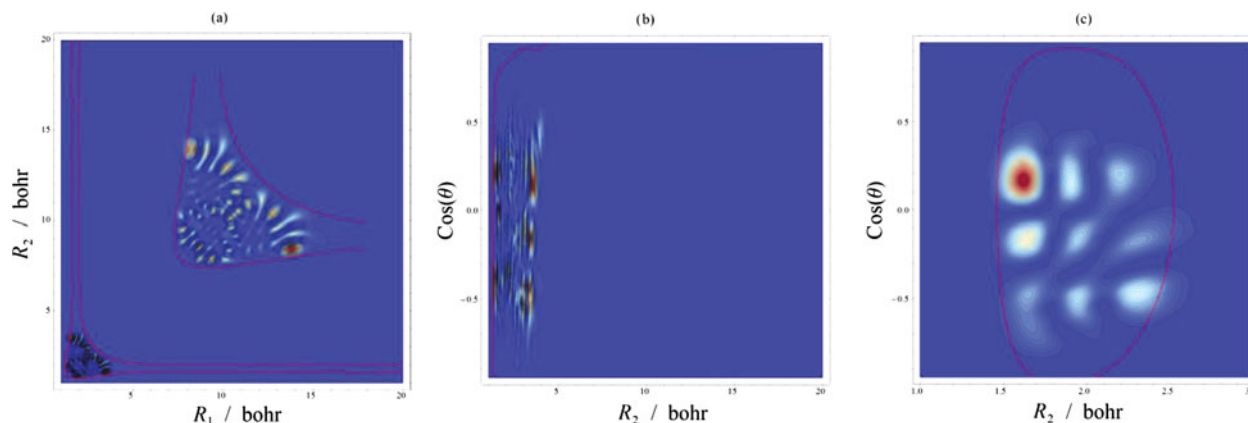
Figure 18.    Two-dimensional sections of the wavefunction corresponding to the $J = 1$ resonance at 41,305 cm$^{-1}$ with $\Gamma = 0.00008$ cm$^{-1}$, obtained by fixing (a) $\mathrm{Cos}(\theta) = 0.2$, (b) $R_1 = 1.9$ Bohr, and (c) $R_1 = 3.5$ Bohr, where $R_1$ and $R_2$ are the two OH bond lengths and $\theta$ is the HOH bond angle. The area near the equilibrium structure is shown enlarged in (a).
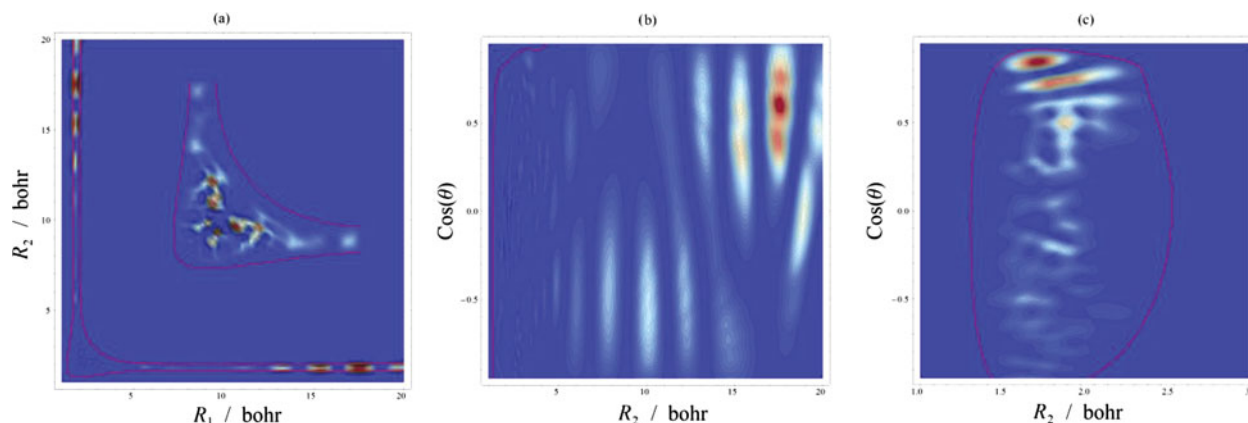


Figure 19.    Two-dimensional sections of the wavefunction corresponding to the $J = 1$ resonance at 41,315 cm$^{-1}$ with $\Gamma = 0.71$ cm$^{-1}$, obtained by fixing (a) $\mathrm{Cos}(\theta) = 0.5$, (b) $R_1 = 1.9$ Bohr, and (c) $R_1 = 3.0$ Bohr, where $R_1$ and $R_2$ are the two OH bond lengths and $\theta$ is the HOH bond angle. The area near the equilibrium structure is shown enlarged in (a).

41,175 and 41,269 cm$^{-1}$, respectively. It is surprising to see a rigid-rotor type effect of the rotation at such high energies for the strongly bound system of H$_2$$^{16}$O. We also note that recent studies show the breakdown of the clear rigid-rotor picture around the barrier to linearity [61]. Thus, the rovibrational resonances at 41,224 and 41,305 cm$^{-1}$ should definitely be called Feshbach resonances. This assignation possibility appears to be a valuable tool to identify at least some rovibrational Feshbach resonances and distinguish them from shape resonances. Finally, it is noted, that the lifetimes of the two $J = 1$ rovibrational Feshbach resonances of Figures 16 and 18 are considerably longer than the lifetimes of their $J = 0$ vibrational counterparts of Figures 3 and 7, respectively.

A systematic and quantitative comparison of rovibrational and vibrational resonance density functions in order to assign rovibrational Feshbach resonances and thus distinguish them from shape resonances might be a fruitful exercise in the future, for which the algorithms and codes developed originally for rovibrational quantum label assignments on the basis of the rigid-rotor decomposition [62] protocol should prove useful.

## 5.    Summary

In this work, an efficient method applicable to the computation of rovibrational resonance states of strongly bound triatomic molecules is developed. The molecule H$_2$$^{16}$O is employed to test the method. The computations are based on constructing the matrix representation of a CCS Hamiltonian on the basis of eigenfunctions obtained from bound-state computations of the system (a subset of all bound states and many additional eigenvectors with corresponding eigenvalues above dissociation are used as a basis during the resonance computations). Bound-state computations are carried out using the D$^2$FOPI code, with which the

CCS method could be effectively merged. This is helped by the fact that the wavefunctions obtained from D$^2$FOPI are partially represented on a DVR basis; thus, the evaluation of the CCS Hamiltonian matrix elements (in particluar the matrix elements of the CCS PES) is straightforward to carry out.

The vibrational resonances of H$_2$$^{16}$O computed via CCS are in good agreement with previous results obtained using the CAP method as long as resonance positions are concerned. Due to the much slower convergence of resonance lifetimes, these often differ substantially. Beyond the identification of new resonances, the CCS results of this study seem to suggest the reassignment of the previously computed resonances.

$J = 1$ rovibrational resonances are also computed in the energy region up to around 210 cm$^{-1}$ above the first dissociation limit. The 74 states found indicate, when compared with the 20 $J = 0$ resonances identified in the same energy region, that shape resonances seem to occur even for the low rotational quantum number of $J = 1$.

Plots of probability density functions computed from CCS wavefunctions are generated and analysed, which result in the following observations: (a) resonance density functions often show a surprisingly simple nodal structure which one expects to see for low-lying bound states; (b) Feshbach resonances can be formed by accumulation of a large amount of energy in either the non-dissociative bending or symmetric streching modes; (c) several types of dissociation behaviour can be identified varying considerably among the states; (d) some rovibrational Feshbach resonances can be found and assigned based on the similarity of their density plots with the $J = 0$ vibrational resonance density plots and (e) the lifetimes of the assigned $J = 1$ rovibrational Feshbach resonances are considerably longer than the lifetimes of their $J = 0$ vibrational counterparts.

Several extensions of the work presented is planned. We plan, for example, to extend our general GENIUSH algorithm [63] with the CCS technique and compute resonance states for systems containing more than three nuclei. This extension would also allow the computation of resonance states of reduced-dimensional models. Further investigation of probability density plots and other type of analyses of the rovibrational wavefunctions of resonance states should shed light on the interesting behaviour of these exotic molecular states.

## Acknowledgements

## References

[1] A.G. Császár, C. Fábri, T. Szidarovszky, E. Mátyus, T. Furtenbacher, and G. Czakó, Phys. Chem. Chem. Phys. **14**, 1085 (2012).
[2] N. Moiseyev, *Non-Hermitian Quantum Mechanics* (Cambridge University Press, Cambridge, 2011).
[3] R. Schinke, *Photodissociation Dynamics* (Cambridge University Press, Cambridge, 1993).
[4] J.R. Taylor, *Scattering Theory* (Wiley, New York, 1972).
[5] R.E. Wyatt and J.Z.H. Zhang, *Dynamics of Molecules and Chemical Reactions* (Marcel Dekker, New York, 1996).
[6] V.I. Kukulin, V.M. Kasnopolsky and J. Horacek, *Theory of Resonances* (Kluwer, Dordrecht, 1988).
[7] A. Bohm, H. Uncu, and S. Komy, Rep. Math. Phys. **64**, 5 (2009).
[8] A. Bohm, Rep. Math. Phys. **67**, 279 (2011).
[9] L.D. Landau and E.M. Lifshitz, *Quantum Mechanics* (Pergamon, Oxford, 1965).
[10] N. Moiseyev, Phys. Rep. **302**, 211 (1998).
[11] T. Carrington, Jr., Can. J. Chem. **82**, 900 (2004).
[12] H. Guo, Rev. Comput. Chem. **25**, 285 (2007).
[13] A.G. Császár, E. Mátyus, T. Szidarovszky, L. Lodi, N.F. Zobov, S.V. Shirin, O.L. Polyansky, and J. Tennyson, J. Quant. Spectr. Rad. Transfer **111**, 1043 (2010).
[14] T. Szidarovszky, A.G. Császár, and G. Czakó, Phys. Chem. Chem. Phys. **12**, 8373 (2010).
[15] O.L. Polyansky, R. Prosmiti, W. Klopper, and J. Tennyson, Mol. Phys. **98**, 261 (2000).
[16] S. Skokov, K.A. Peterson, and J.M. Bowman, J. Chem. Phys. **109**, 2662 (1998).
[17] A.G. Császár, W.D. Allen, Y. Yamaguchi, and H.F. Schaefer III, *Computational Molecular Spectroscopy* (Wiley, Chichester, 2000).
[18] N.C. Handy, Y. Yamaguchi, and H.F. Schaefer III, J. Chem. Phys. **84**, 4481 (1986).
[19] B.T. Sutcliffe, J. Chem. Soc. Faraday Trans. **89**, 2321 (1993).
[20] B.T. Sutcliffe and J. Tennyson, Int. J. Quant. Chem. **39**, 183 (1991).
[21] J.C. Light and T. Carrington, Adv. Chem. Phys. **114**, 263 (2000).
[22] T. Szidarovszky, Ph. D. dissertation, Eötvös University, Budapest, Hungary, 2012.
[23] U.V. Riss and H.-D. Meyer, J. Phys. B: At. Mol. Opt. Phys. **26**, 4503 (1993).
[24] W.P. Reinhardt, Annu. Rev. Phys. Chem. **33**, 223 (1982).
[25] Y.K. Ho, Phys. Rep. C **99**, 1 (1983).
[26] J. Aguilar and J.M. Combes, Commun. Math. Phys. **22**, 269 (1971).
[27] E. Balslev and J.M. Combes, Commun. Math. Phys. **22**, 280 (1971).
[28] B. Simon, Commun. Math. Phys. **27**, 1 (1972).
[29] M. Reed and B. Simon, *Methods of Modern Mathematical Physics*, Vol. 4: Analysis of Operators (Academic Press, London, 1972).
[30] N. Rom and N. Moiseyev, J. Chem. Phys. **99**, 7703 (1993).
[31] N. Moiseyev and J.O. Hirschfelder, J. Chem. Phys. **88**, 1063 (1988).
[32] V V. Ryaboy and N. Moiseyev, J. Chem. Phys. **103**, 4061 (1995).
[33] V. Ryaboy, N. Moiseyev, V.A. Mandelshtam, and H.S. Taylor, J. Chem. Phys. **101**, 5677 (1994).
[34] S.I. Chu, J. Chem. Phys. **72**, 4772 (1980).
[35] S. Skokov, J.M. Bowman, and V.A. Mandelshtam, Phys. Chem. Chem. Phys. **1**, 1279 (1999).

[36] B. Poirier and T. Carrington Jr., J. Chem. Phys. **116**, 1215 (2002).

[37] H.Y. Mussa and J. Tennyson, Chem. Phys. Lett. **366**, 449 (2002).

[38] J.C. Tremblay and T. Carrington Jr., J. Chem. Phys. **122**, 244107 (2005).

[39] B.C. Silva, P. Barletta, J.J. Munro, and J. Tennyson, J. Chem. Phys. **128**, 244312 (2008).

[40] M. Grechko, P. Maksyutenko, T.R. Rizzo, and O.V. Boyarkin, J. Chem. Phys. **133**, 081103 (2010).

[41] H.Y. Mussa and J. Tennyson, J. Chem. Phys., **109**, 10885 (1998).

[42] O.L. Polyansky, A.G. Császár, S.V. Shirin, N.F. Zobov, P. Barletta, J. Tennyson, D.W. Schwenke and P.J. Knowles, Science, **299**, 539 (2003).

[43] G. Li and H. Guo, J. Molec. Spectrosc., **210**, 90 (2001).

[44] N.F. Zobov, S.V. Shirin, L. Lodi, B.C. Silva, J. Tennyson, A.G. Császár, and O.L. Polyansky, Chem. Phys. Lett. **507**, 48 (2011).

[45] C.G.J. Jacobi, Cr. Hebd. Acad. Sci. **15**, 236 (1842).

[46] B.T. Sutcliffe and J. Tennyson, Int. J. Quant. Chem. **39**, 183 (1991).

[47] J. Tennyson and B.T. Sutcliffe, J. Chem. Phys. **77**, 4066 (1982)

[48] C. Leforestier, J. Chem. Phys. **94**, 6388 (1991).

[49] R.N. Zare, *Angular Momentum* (Wiley, New York, 1988).

[50] H. Wei and T. Carrington Jr., J. Chem. Phys. **97**, 3031 (1992).

[51] J. Echave and D.C. Clary, Chem. Phys. Lett. **190**, 225 (1992).

[52] V. Szalay, G. Czakó, Á. Nagy, T. Furtenbacher, and A.G. Császár, J. Chem. Phys. **119**, 10512 (2003).

[53] C. Lanczos, J. Res. Natl. Bur. Stand. **45**, 255 (1950).

[54] J.K. Cullum and R.A. Willoughby, *Lanczos Algorithms for Large Symmetric Eigenvalue Computations* (Birkhauser, Boston, 1985).

[55] Y. Saad, *Iterative Methods for Sparse Linear Systems* (Society for Industrial and Applied Mathematics, Philadelphia, PA, 2003).

[56] N. Moiseyev, S. Friedland, and P.R. Certain, J. Chem. Phys. **74**, 4739 (1981).

[57] G. Tarczay, A.G. Császár, W. Klopper, and H.M. Quiney, Mol. Phys. **99**, 1769 (2001).

[58] P. Maksyutenko, T.R. Rizzo, and O.V. Boyarkin, J. Chem. Phys. **125**, 181101 (2006).

[59] P.D. Chowdary and M. Gruebele, Phys. Rev. Lett. **101**, 250603 (2008).

[60] P.D. Chowdary and M. Gruebele, J. Chem. Phys. **130**, 024305 (2009).

[61] T. Szidarovszky, C. Fábri, and A.G. Császár, J. Chem. Phys. **136**, 174112 (2012).

[62] E. Mátyus, C. Fábri, T. Szidarovszky, G. Czakó, W.D. Allen, and A.G. Császár, J. Chem. Phys. **133**, 034113 (2010).

[63] E. Mátyus, G. Czakó, and A.G. Császár, J. Chem. Phys. **130**, 134112 (2009); C. Fábri, E. Mátyus, and A.G. Császár, J. Chem. Phys. **134**, 074105 (2011).